

pubs.acs.org/cm Article

Spectroelectrochemical Network Measurements for Redox Bioelectronics

Zhiling Zhao, Eunkyoung Kim, Dana Motabar, William E. Bentley, and Gregory F. Payne*



Cite This: Chem. Mater. 2023, 35, 976-990



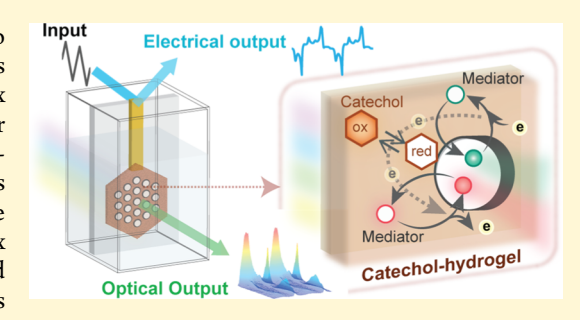
ACCESS I

III Metrics & More

Article Recommendations

Supporting Information

ABSTRACT: Redox bioelectronics enlists electrochemical methods to connect to biology through biology's native redox modality. The activities of this redox modality involve the exchange of electrons through redox reactions, and often, individual redox reactions are embedded within larger redox-reaction networks. Here, we examined electrodes coated with redox-active but non-conducting catechol-containing hydrogels that are emerging as important materials in redox-based bioelectronics. Previous studies have shown that electron "flow" through these catechol hydrogels involves redox reactions, and in some cases, catechol's redox-state switching can be observed by orthogonal electrical and optical measurements. Here, we extend analysis by increasing the dimensionality of dynamic optical measurements from a



single wavelength to a broader spectrum and adapt a minimal deterministic network model to reveal the intrinsic structure of this additional data. This increased dimensionality enhances our capabilities for detecting and interpreting discriminating signals, and we demonstrate these capabilities by comparing the response characteristics of conducting versus redox-active hydrogels and redox networks with different topologies. We discuss the importance of increasing measurement dimensionality to enhance both data-driven and theory-guided approaches for information processing in redox-based bioelectronics.

■ INTRODUCTION

There are diverse efforts to interface biology and electronics to address some of the world's most pressing technological challenges that include the recovery of energy from sustainable resources (e.g., microbial fuel cells¹); the manufacture of environmentally friendly chemicals and materials (e.g., electrobiofabrication² and electrobiotechnology³,⁴); and the precision targeting of interventions in complex medical or environmental systems (e.g., electrogenetics⁵-7). In many of these examples, the interconnection between biology and electronics involves redox reactions. Redox is a native modality used by biology for energy harvesting (respiration), biosynthesis, and communication (redox signaling), and redox is also accessible to electronics via electrochemistry. Our focus is redox-based bioelectronics.^{8,9}

In conventional bioelectronics, electrodes often "connect" through biology's ion-based electrical modality that is common for signaling in the nervous, neuromuscular, and cardiovascular systems. This interfacing to biology's ionic electrical modality has been remarkably successful both for studying molecular/cellular mechanisms (e.g., voltage-gated ion channels) and for sensing/actuating at a system level (e.g., electrocardiograms, EKGs, and defibrillators can detect and correct life-threatening arrythmias). The emerging redox bioelectronics aims to connect to biology through its electron-based redox modality that is integral to signaling in the immune system and among cells in complex ecosystems (e.g., gut microbiome or soil rhizosphere). Table 1 provides a comparison between the

ion-based electrical modality and the electrical features of the redox modality. ¹⁴ From an electronics perspective, the redox modality involves the "flow" of electrons through redox reactions (not the flow of ions across membranes), ^{15–19} and this has profound effects on the signals that can be measured (or imposed) and how the signals are measured and analyzed.

Current research in redox bioelectronics often enlists five somewhat specialized approaches in electrochemistry. First, electrodes are used to provide system-level measurements. This approach essentially uses the electrode as a pseudosensory organ to discern differences: while these differences result from the underlying chemistry, the goal is to discern robust system-level features but not to map features to the chemical composition and concentration. This approach is analogous to the electrocardiogram (EKG) where the critical information is contained in the system-level pattern and not in how this pattern maps to lower-level activities (i.e., the clinical value of the EKG does not require mapping to the number and types of ions crossing individual membrane channels).

Received: September 3, 2022 Revised: January 6, 2023 Published: January 17, 2023





Table 1. Comparison of the Electrical Features of the Redox Modality and the Ion-Based Electrical Modality (the Statements Are Generalizations and May Not Be Absolutely True in All Cases)^a

	redox modality	ion-based electrical modality
signal	reactive molecules (e.g., reactive oxygen; ROS)	ion-based activities (e.g., action potentials)
"charge carrier"	electron	ion
charge carrier solubility?	no (electrons "shuttled" by molecules)	yes (ions are soluble)
mechanism of current flow	electron-transfer reaction (change in the redox state)	ion flow across the membrane (change in the ion position)
driving force for current flow	redox potential difference	electrochemical membrane gradient
constraints on current flow	kinetic barriers (activation energies)	physical barriers (membranes)
enabling mechanisms	enzymes	membrane-spanning channels
example of the signal reception mechanism	sulfur switching (oxidation of protein cysteines to disulfides)	voltage-gated ion channels

^aAdapted with permission from ref 14. Copyright 2021 American Chemical Society.

Second, diffusible mediators are often used to overcome kinetic barriers and to target less-accessible redox-active species (e.g., insoluble materials²¹), buried active sites of enzymes, ^{22,23} or intracellular activities. ^{24,25} To circumvent the well-known limitations of electrochemistry (e.g., electrode fouling) and mediators (e.g., ligand exchange), signal analysis in redox bioelectronics is often performed after measurements have stabilized, and conclusions are often based on comparisons against control measurements. ²⁶

Third, optical measurements are coupled with electrical measurements to provide complementary information. In general, the coupling of orthogonal spectroscopic and electrochemical measurements is beneficial because the former provides structural/chemical information, while the latter provides kinetic/activity information.^{27–30} For redox bioelectronics, optical measurements can be especially useful because the absorption spectra often depend on the redox state, and thus, optical measurements can provide information of the redox-state switching. Furthermore, optical and electrical measurements are device-compatible and miniaturizable, thus offering the potential for sensor fusion in portable devices.

Fourth, the starting point for quantitative analysis in redox bioelectronics is electrochemical reaction-diffusion models that are commonly used for bottom-up analysis of simple electrochemical systems (e.g., to determine reaction mechanisms).^{31–34} As the number of interacting redox species increases, schematics for these reaction-diffusion models begin to resemble reaction networks with the individual reacting species being network nodes and the node-node electron-transfer reactions being network links. It is envisioned that such deterministic models will become less tractable as the number of nodes (and model parameters) increases and also if the structure of the redox network is unknown (e.g., a biological redox interactome may have unknown nodes and links). It is envisioned that with greater complexities and uncertainties, physics-based deterministic models will require abstractions with the goal shifting from creating a digital replica of the redox reactions to identifying characteristic system-level behavior of the redox network. The use of reaction—diffusion and network models as the quantitative framework in redox bioelectronics is fundamentally different from the use of electrical circuit models in electrochemical impedance spectroscopy and ion-based bioelectronics (e.g., Hodgkin—Huxley model).

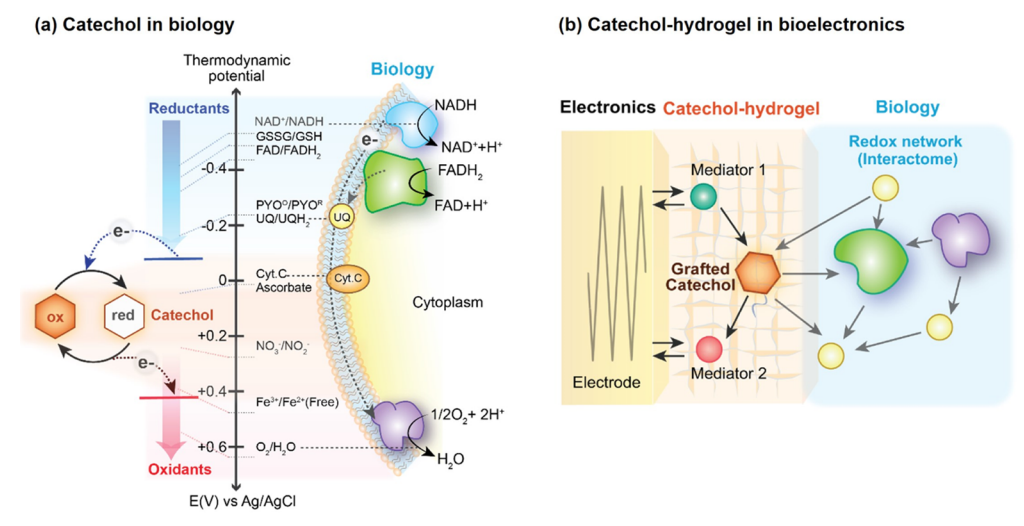
Fifth, catechols are emerging as important molecular components in redox bioelectronics. 35-39 From a biological perspective, catechols have redox potentials in the midphysiological range and can spontaneously donate to and accept electrons from a wide range of reductants and oxidants as suggested in Scheme 1a. Catechol's redox properties can be accessed for bioelectronics by coating electrodes with catecholcontaining hydrogel films that are redox-active but nonconducting (i.e., the film's catechol moieties can donate to and accept electrons from diffusible mediators but cannot directly exchange electrons with the electrode). 35,40 As illustrated in Scheme 1b, these hydrogel-embedded catechol nodes can serve as "hubs" that are capable of spanning redox-based "communication" between biology and electronics. 41,42 Recent studies have shown that the redox state of catechol hydrogels can be readily measured optically (due to its redox-statedependent absorbance),³⁶ and also, a minimal reactiondiffusion model (without parameter optimization) can reveal the intrinsic structure of the data describing the flow of electrons and molecular switching of the catechol hydrogel.⁴³ It is interesting to note that while catechol can be functionally described as a two-state molecular memory (quinonecatechol), its switching involves two electrons, and the two states are separated by an unstable intermediate state (semiquinone), and the memory states are stable for hours to days.36

Here, we extend analysis in two important ways. First, as illustrated in Scheme 1c, we extend the dimensionality of the optical measurements from detecting the redox-state switching of the catechol node to detecting switching of the diffusible mediator nodes. Specifically, we extend measurement from a transparent electrode to a honeycomb electrode in which the absorbance measurements in the optical window detect the redox state of the diffusible nodes. Furthermore, these optical measurements were not confined to a single wavelength but were collected over the broader UV-vis spectrum (from 300 to 800 nm). Second, we extend the deterministic minimal network model to reveal the intrinsic structure of these mediator-based optical measurements. We demonstrate that these measurements could discern the differences between the networked flow of electrons through a catechol film and the conductivity-based flow of electrons through a graphene film. Furthermore, we demonstrate that the high-dimensional measurements could detect network-topology-dependent signal differences. We believe that this work contributes to addressing an overarching challenge in bioelectronics: to increase the information content of simple, rapid, and miniaturizable electrode measurements.

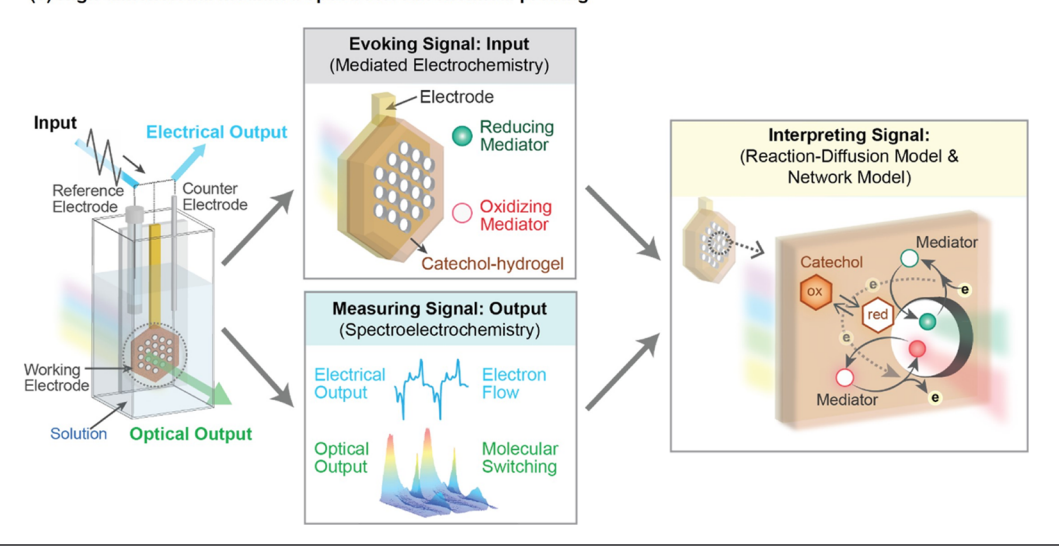
■ EXPERIMENTAL SECTION

Materials. Chitosan, catechol, phenazine-1-carboxylic acid, 1,1-ferrocenedimethanol, paraquat, and $K_3 IrCl_6$ were purchased from Sigma-Aldrich. Graphene (N002-PDR) was purchased from Angstron Materials (Dayton, OH). All reagents were used as received without further purification. All solutions were prepared using Millipore water (>18 $\,\mathrm{M}\Omega)$. The solutions of mediators were prepared in 0.1 M phosphate buffer (pH 7.0) with air being excluded by purging N_2 before the experiment.

Scheme 1. (a) Catechol Moieties Can Exchange Electrons with Various Biological Reductants and Oxidants, (b) Hydrogel-Embedded Catechol Moieties Can Serve as Hubs for the Networked Flow of Electrons between Biological and Electronic Systems, and (c) Spectroelectrochemical Measurement Can Acquire High-Dimensional Data of the Redox-State Switching of Network Nodes (e.g., Diffusible Mediators)



(c) High dimensional mediated spectroelectrochemical probing



Instrumentation. The spectroelectrochemical cell consisted of a honeycomb gold (19 holes of 0.5 mm diameter from Pine Research) working electrode, a AglAgCl reference electrode, and a counter electrode made of a 0.3 mm platinum wire. A potentiostat (CHI 620, CH Instruments) was used for the electrofabrication of hydrogel films and all the electrochemical measurements. A UV—vis spectrophotometer (AvaSpec-ULS2048, Pine Research) was used for the spectral measurements which were carried out simultaneously with the electrochemical measurements.

■ RESULTS

Spectroelectrochemical Measurement. To enable the simultaneous measurement of electrical and optical responses, we used the honeycomb electrode of Scheme 1c.^{21,44} Specifically, this gold electrode is perforated with a honeycomb pattern of holes (19 holes of 0.5 mm diameter) that serve as an "optical window" for spectral measurement of the redox-state switching of the diffusible mediators. Although these electrodes offer good within-sample reliability, there can be considerable between-sample variability because of variabilities in electrode's electrochemically active surface area and the exact positioning of the electrode within the cuvette. In experiments

in which we compared the performance of different film coatings, we used honeycomb electrodes that were observed to have comparable active-surface areas as measured by methods described in Figure S1 of the Supporting Information.

Electrical Response Characteristics of Conducting and Redox-Active Hydrogels. In initial studies, we compared the response characteristics of honeycomb electrodes coated with either a catechol-containing or graphenecontaining hydrogel film. These films were electrodeposited on the electrode surface using the pH-responsive film-forming aminopolysaccharide chitosan and previously described methods. 43 Briefly, the graphene-chitosan film was electrofabricated by co-deposition from a suspension containing graphene (1% w/v) and chitosan (~1% w/v, pH 5.5) using a cathodic potential (-1.4 V vs Ag/AgCl, 2 min). The catechol chitosan film was electrofabricated in two steps: first, a chitosan hydrogel film was electrodeposited from a chitosan solution (\sim 1% w/v, pH 5.5) using a cathodic potential (-1.4V vs Ag/AgCl, 2 min), and then, the chitosan-coated electrode was immersed into a catechol solution (5 mM), and an anodic potential +0.5 V was applied for ~ 2.5 min to achieve an anodic

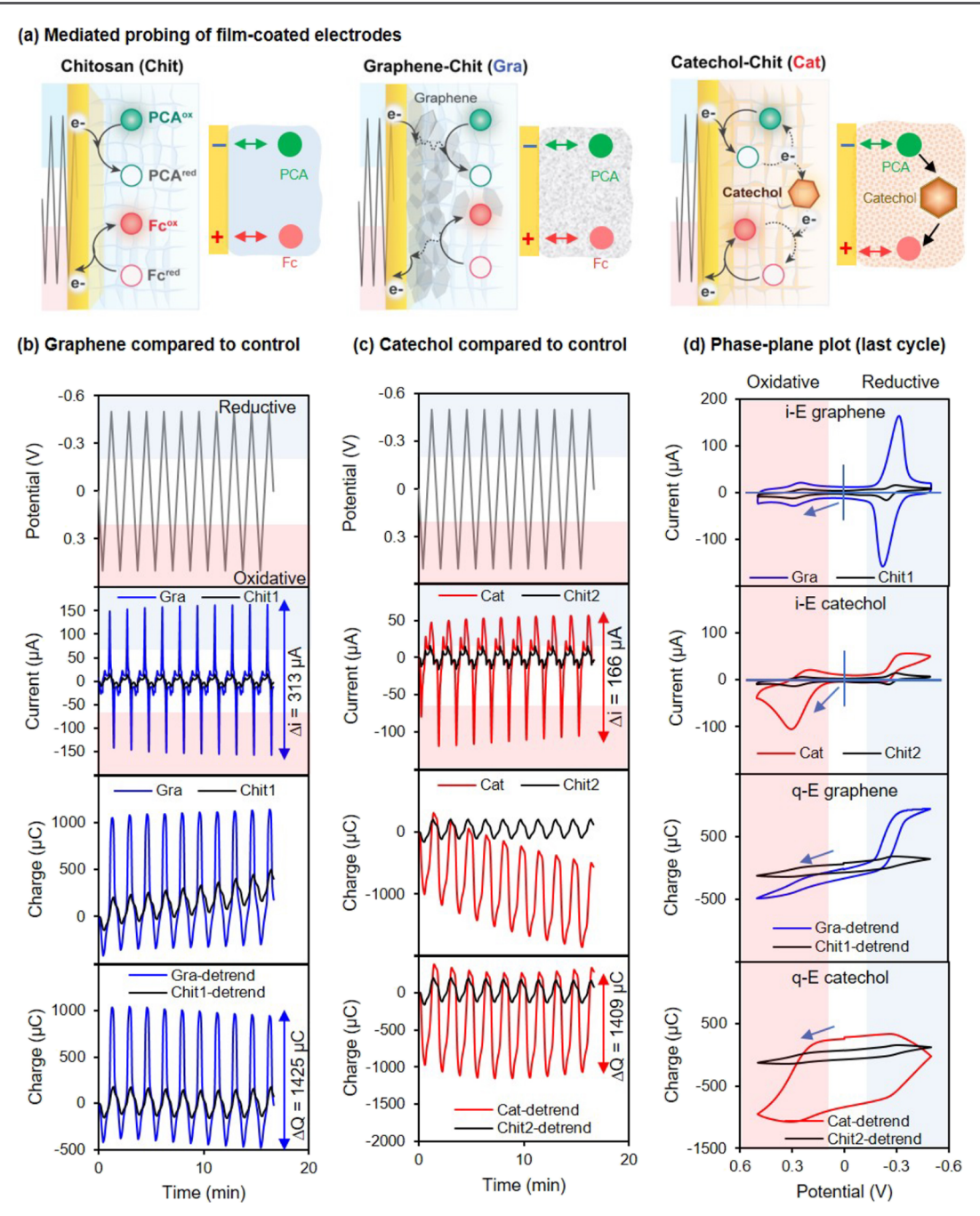


Figure 1. Electrical response characteristics for electrodes coated with graphene—chitosan and catechol—chitosan films. (a) Schematic illustrations of the electron transfer reactions and the network interaction graphs for the three film-coated honeycomb electrodes. (b) Input—output time series comparison for the graphene—chitosan film and an equivalent chitosan control film (Chit1). (c) Input—output time series comparison for the catechol—chitosan film and an equivalent chitosan control film (Chit2). (d) Phase plane plots show differences in the current (i) and charge (q) responses to the imposed potential (E), while the arrows indicate the direction of scanning. Note: the honeycomb electrode area for the control Chit1 (81 mm²) was similar to that for the graphene—chitosan-coated electrode (79 mm²) while that for the control Chit2 (87 mm²) was similar to that for the catechol—chitosan-coated electrode (85 mm²).

charge transfer (qfab) of 20 mC (Figure S2 of the Supporting Information provides further details of film fabrication).

To characterize the electrical properties, these film-coated electrodes were immersed into a solution containing two mediators: the bacterial metabolite phenazine-1-carboxylic acid (PCA; 0.1 mM; $E^0 = -0.25$ V vs Ag/AgCl) which is believed to participate in a two-electron transfer reaction⁴⁵ and a standard electrochemical mediator ferrocene dimethanol (Fc; 0.2 mM; $E^0 = +0.25$ V vs Ag/AgCl) that is believed to

participate in a one-electron transfer reaction. A cyclic oscillating input potential between +0.5 and -0.5 V (vs Ag/AgCl; scan rate = 20 mV/s) was then imposed onto the underlying electrode as shown in Figure 1a which also illustrates both the electron transfer reactions and relevant network interaction graphs.

In initial studies, we performed multi-cycle cyclic potential input—output time series studies and compared the response characteristics with those of equivalent control chitosan films.

The output current for the graphene—chitosan film shown in Figure 1b shows oscillations that are nearly steady (time-invariant); amplitudes ($\Delta i = 313~\mu A \pm 7$) that are large compared to those of the control chitosan film (Δi of 30 $\mu A \pm 0.3$); and amplifications in both oxidation and reduction compared to the control chitosan film. The amplified currents for the graphene—chitosan film (compared to those for the equivalent control chitosan film Chit1) are consistent with the explanation that the hydrogel-entrapped graphene serves to enhance the conducting surface area and possibly also confers electrocatalytic activities.

The second set of output curves shown in Figure 1b are for charge ($q=\int i\ dt$). The charge output for the graphene—chitosan film is also oscillating and amplified (compared to that for the control chitosan film). The output charge for both films shows a slight trend over time, and after detrending (using the "detrending" function of Signal Processing Toolbox of MATLAB), the lower curve shown in Figure 1b shows both outputs appearing steady with amplitudes $\Delta q=1425\ \mu\text{C}\pm2$ for the graphene—chitosan and $\Delta q=301\ \mu\text{C}\pm10$ for the control chitosan film.

Figure 1c shows the output curves for electrodes coated with the catechol–chitosan film and an equivalent chitosan control film (Chit2). The output current for the catechol–chitosan film shown in Figure 1c shows oscillations that are nearly steady (time-invariant); amplitudes ($\Delta i = 166~\mu A \pm 2.5$) that are large compared to those of the control chitosan film ($\Delta i = 30~\mu A \pm 0.4$); and large amplifications in oxidation and smaller amplifications in reduction. Possibly, the smaller current amplifications in reduction reflect the lower reactivity of PCA relative to Fc. The output charge for the catechol–chitosan film shows a significant trend in the oxidative direction but after detrending shows comparatively large amplitude oscillations ($\Delta q = 1409~\mu C \pm 7$) compared to those for the control chitosan film ($\Delta q = 304~\mu C \pm 6$).

Although the input—output time series curves show amplified currents and charge for both the graphene and catechol films (compared to those for control chitosan films), the differences in response characteristics between graphene and catechol are more apparent from their phase plane plots. The current—potential (i–E) phase plane plot shown in Figure 1d for the graphene—chitosan film shows peak currents in the potential regions for the PCA and Fc mediators, and amplification is observed (compared to that for the control chitosan film) in both the reduction and oxidation directions for each mediator.

The charge-potential (q-E) phase plane plots shown in Figure 1d are helpful for providing mechanistic insights into these electrical response characteristics of the films. The response characteristics for the graphene-chitosan film are consistent with the reversible electrochemical reactions of the PCA and Fc mediators that are amplified due to the higher active electrochemical surface area conferred by graphene. When the imposed potential becomes more reducing (i.e., more negative) than PCA's E^0 (-0.25 V), electrons are transferred to switch PCA^{ox} into PCA^{red}, but this PCA^{red} is reoxidized when the potential is subsequently cycled to more oxidative (i.e., positive) potentials. Similarly, when the imposed potential is cycled to become more oxidative than Fc's E^0 (+0.25 V), electrons are transferred to switch Fc^{red} into Fcox, but this Fcox is re-reduced as the potential is cycled to become more reducing.

The i-E phase plane plot for the catechol-chitosan film shown in Figure 1d shows a markedly different pattern: in the PCA potential region, reduction currents are greatly amplified, while oxidation currents are not amplified; and in the Fc potential region, oxidation currents are greatly amplified, but reduction currents are only slightly amplified. This current response is consistent with the network interaction graph in the rightmost schematic shown in Figure 1a in which the reduced PCA (PCA^{red}) and the oxidized Fc (Fc^{ox}) can engage in directed electron transfer reactions with the catechol node. Mechanistically, when the imposed potential becomes reducing and PCAox is switched into PCAred, PCAred can diffuse into the hydrogel and transfer its electrons to the catechol. This electron transfer between PCAred and Catox re-oxidizes the PCA—thus, when the imposed potential is then cycled into the oxidative region, there is less PCAred available to donate electrons to the electrode (i.e., a small oxidative current is observed in the PCA potential region). Similarly, when the imposed potential becomes more oxidizing and Fcred is switched into Fcox, Fcox can diffuse into the hydrogel and accept electrons from catechol. This electron transfer between Fcox and Catred re-reduces Fc—thus, when the imposed potential is then cycled into the reductive region, there is less Fcox available to accept electrons from the electrode (i.e., a small reductive current is observed in the Fc potential region).

The charge-potential (q-E) phase plane plot shown in Figure 1d for the catechol-chitosan film is markedly different from that for the graphene-chitosan film. Specifically, this q-E phase plane plot is consistent with the interpretation that at potentials where PCA can be electrochemically reduced, electrons are donated (via PCA^{red}) to the film's catechol moieties where they are stored. The electrons are stored in the catechol node (i.e., as Cat^{red}) until the potential is cycled to values sufficiently oxidative for Fc to be switched to its oxidized state which can then accept electrons from film's Cat^{red}. In essence, the mediators serve to gate the flow of electrons into the film (via PCA) or out of the film (via Fc).

Subtleties Associated with the Networked Flow of **Electrons.** Figure 1 demonstrates that there are significant mechanistic differences in the way in which electrons flow through conducting or redox-active films, and it is useful to consider a couple of subtleties associated with the networked flow of electrons within the catechol-chitosan film. First, most mediators have low barriers for electron transfer and thus tend to react spontaneously: thus, initially, the mediators are typically in an inert redox state prior to imposing the potential inputs that initiate redox probing. For the example shown in Figure 1, the PCA is initially in its oxidized state (PCAox) and lacks donatable electrons for interacting with catechol. Only when the electrode is cycled to a sufficiently reducing potential does the PCA reduces to its "active" PCAred state capable of donating electrons to catechol. Similarly, the initial Fc^{red} state is inactive and requires an oxidative electrode potential to be activated into its Fcox state. Thus, the flow of electrons between nodes is constrained by thermodynamics but also depends on the redox states of the nodes that are participating in the electron transfer reactions. As will be discussed later, the active forms of mediators (e.g., PCA^{red} and Fc^{ox}) could exchange electrons with each other; however, this does not occur in this case because these active forms do not co-exist at the same time in the same location.

Second, the optical properties (e.g., absorbance) of many molecules (e.g., nodes) depend on their redox state. Thus, the

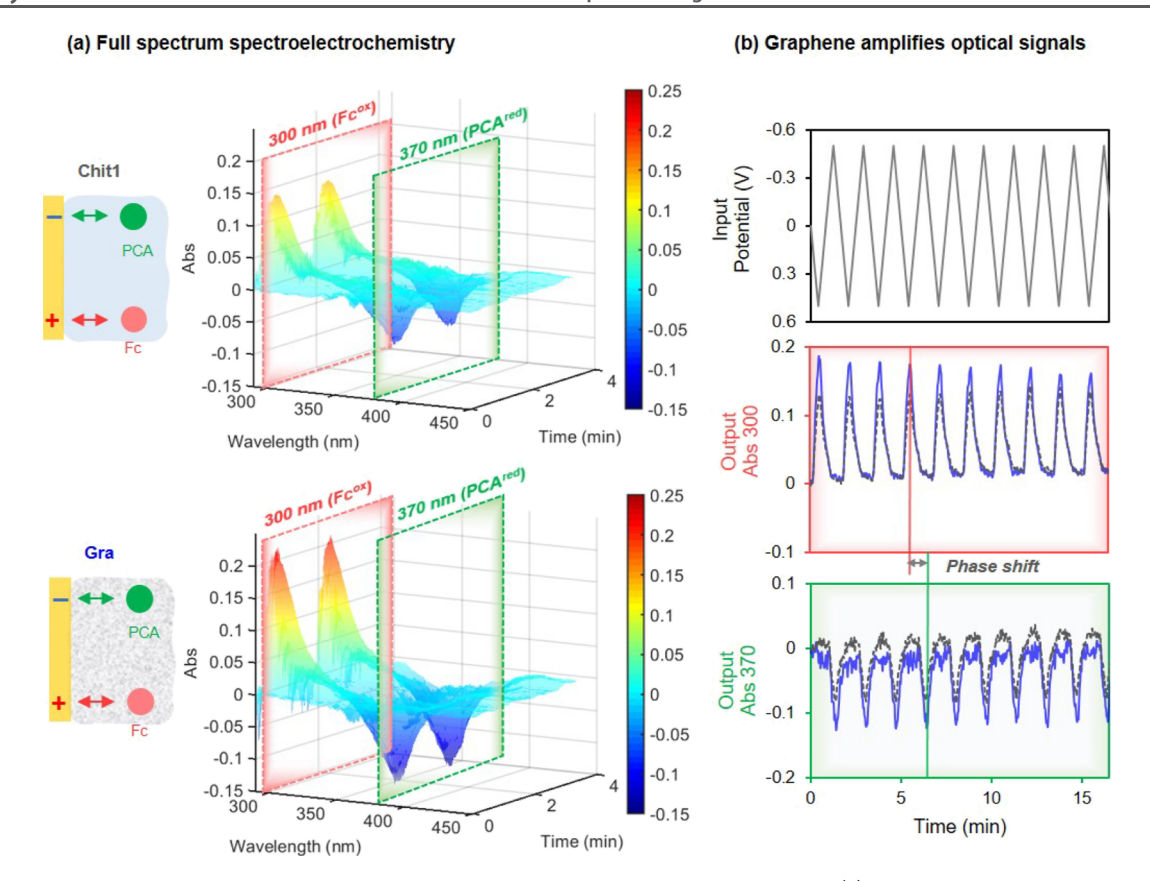


Figure 2. Optical response characteristics for electrodes coated with the graphene—chitosan film. (a) Three-dimensional plot showing optical absorbance as a function of the wavelength and time while a cyclically oscillating input potential was imposed onto the underlying electrode: the differential spectra show peaks at 300 nm and 370 nm which are primarily due to the generation of Fc^{ox} and PCA^{red} , respectively. (b) Two-dimensional time series plots of input potential and output absorbances at 300 and 370 nm. Note: the optical response characteristics shown here were obtained in the same experiment as that of the electrical response characteristics shown in Figure 1 (potential scan rate 20 mV/s; spectrum measurement every 2 s).

motivation for fusing electrical and optical measurements is that the electrical measurements characterize the network's activity (i.e., flow of electrons), while the optical measurements provide molecular-level information of a node's redox-state switching. Ideally, these two measurements offer complementary information: the dynamic flow of electrons through the network that is measured electrically should be correlated to the redox-state switching of the individual or collection of nodes that are measured optically. The opportunity to simultaneously measure multiple wavelengths (or an entire spectrum) during redox probing offers the possibility to meaningfully increase the dimensionality of the observable output response characteristics.

Optical Response- Characteristics of Conducting and Redox-Active Hydrogels. In the same experiment in which the electrical response characteristics were measured (i.e., Figure 1), we also characterized the optical responses. Specifically, we collected time-dependent spectra every 2 s over the broad wavelength range of 300–800 nm as illustrated in Scheme 1c. For visualization, we report differential spectra in which the spectrum measured in the initial mediator solution (i.e., with "inert" PCA^{ox} and Fc^{red}) was used as a reference that was subtracted from the spectrum collected at each time point.

Figure 2 compares the optical absorbance output response for the graphene—chitosan film and a control chitosan film. The three-dimensional plots shown in Figure 2a show the

wavelength, scanning time, and absorbance for two cycles of cyclic voltammetry (CV) measurements, and these plots show that two sets of absorbance "peaks" are observed. The maxima at 300 nm correspond to the absorbance for activated Fc^{ox}, while the minima at 370 nm correspond to the absorbance of activated PCA^{red} (see Figure S3 of the Supporting Information for further details of the absorbance peaks). Both absorbance peaks are amplified for the graphene—chitosan film (compared to those for the control chitosan film).

Figure 2b shows two-dimensional representations as potential input and absorbance outputs at 300 nm (Fcox) and 370 nm (PCA^{red}) over the entire 10 cycles of the experiment. There are three observations from these inputoutput time series representations. First, the peaks at 300 nm and 370 nm are out-of-phase with each other. This means that the active forms of the Fcox and PCAred mediators are generated at different times and do not appear to co-exist in the same location at the same time. This observation is consistent with the network interaction graph illustrated in Figure 1a in which no links are shown to connect the Fc and PCA mediators. Second, the optical outputs appear reasonably steady over time, consistent with reversible electrochemical reactions of the Fc and PCA mediators. Finally, both peak absorbances are amplified for the graphene-chitosan film (compared to those for the control chitosan film), and this observation is consistent with the amplified currents observed

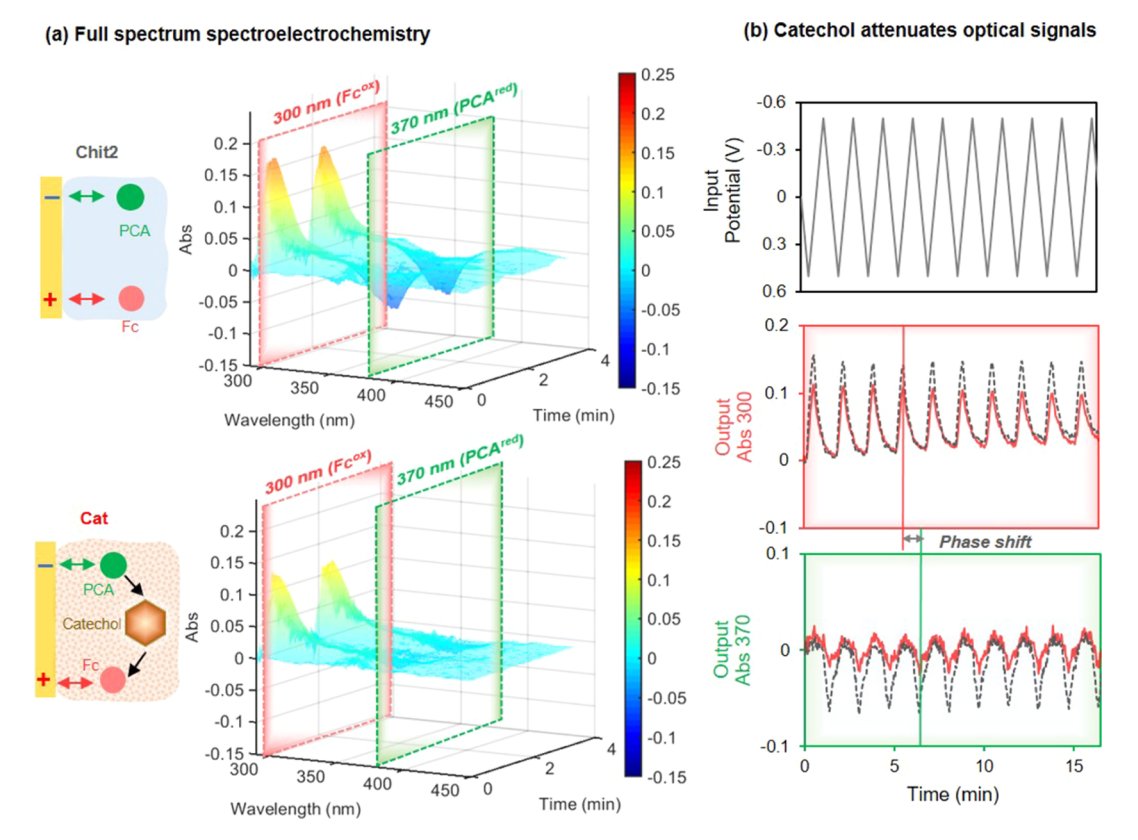


Figure 3. Optical response characteristics for electrodes coated with the catechol—chitosan film. (a) Three-dimensional plot of absorbance, wavelength, and time during a cyclically imposed input potential. (b) Two-dimensional time series plots of input potential and output absorbance at 300 and 370 nm. Note: the optical response characteristics shown here were obtained in the same experiment as that of the electrical response characteristics shown in Figure 1 (potential scan rate 20 mV/s; spectrum measurement every 2 s).

in Figure 1b which suggests a greater rate of generation of the active forms of the mediators.

Analogous three-dimensional plots and optical input—output curves are shown in Figure 3 for the catechol-chitosan films. As observed for the graphene-chitosan films, oscillating absorbance peaks for the catechol-chitosan films are observed at 300 nm (Fcox) and 370 nm (PCAred); the peaks are out of phase with each other, and the peaks appear nearly steady over time. In contrast to those for the graphene-chitosan film, the optical absorbances at 300 and 370 nm for the catecholchitosan films are attenuated relative to an equivalent chitosan control film. Such attenuations in mediator optical absorbance have been observed before 46 with catechol-chitosan films and have been attributed to mediator-catechol electron-exchange reactions that decrease the local concentrations of the activated mediator (i.e., the observed absorbance reflects the balance between the generation of the activated mediator at the electrode and its consumption by interactions with the catechol node).

Extending the Minimal Model to the Mediators' Redox-State Switching. Our long-term vision is to develop mediated electrochemical probing (MEP) as a tool for redox-based bioelectronics. For instance, we envision using mediators and electrical inputs to evoke measurable output responses from samples with complex and ill-defined redox networks and to use the response characteristics to extract meaning (e.g., to probe clinical serum samples to detect meaningful signatures of oxidative stress). ^{26,47} A key aspect of this vision is feature engineering: to discern how observable measurements can be transformed into quantitative metrics

(i.e., features or descriptors) that can be used to reveal meaningful patterns. For instance, key features of an EKG are peak heights and peak positions, and these features are used by clinicians to assess cardiovascular health. Although empirical data-driven (i.e., statistical) approaches are often used for feature engineering, we are investigating a theory-guided approach.⁴³

Specifically, we are using a standard software package (electroanalysis interface of COMSOL) to create a physicsbased minimal model that can be used for theory-guided feature engineering (see Figure S4 of the Supporting Information for details). Specifically, the goals of the model are to discern the intrinsic patterns in the data and identify measurable features (e.g., signal metrics) that can be generally applied for characterization.⁴³ This deterministic model incorporates three mechanistic phenomena: electrochemical reactions (i.e., electrode-node reactions); mediator diffusion; and electron exchange between the mediators and catechol (node-node interactions). The model ignores many phenomena that are presumably of secondary importance in revealing the data's intrinsic structure. Specifically, we did not adapt the model or optimize model parameters to account for differences in the electrode material or geometry; differences in reactivities (we equated rate constant values for all electrode-node interactions and node-node interactions); and time-dependent behavior associated with mediator deactivation (e.g., ligand exchange) and/or electrode fouling (note: the COMSOL report in the Supporting Information provides further details and parameter values for these simulations).

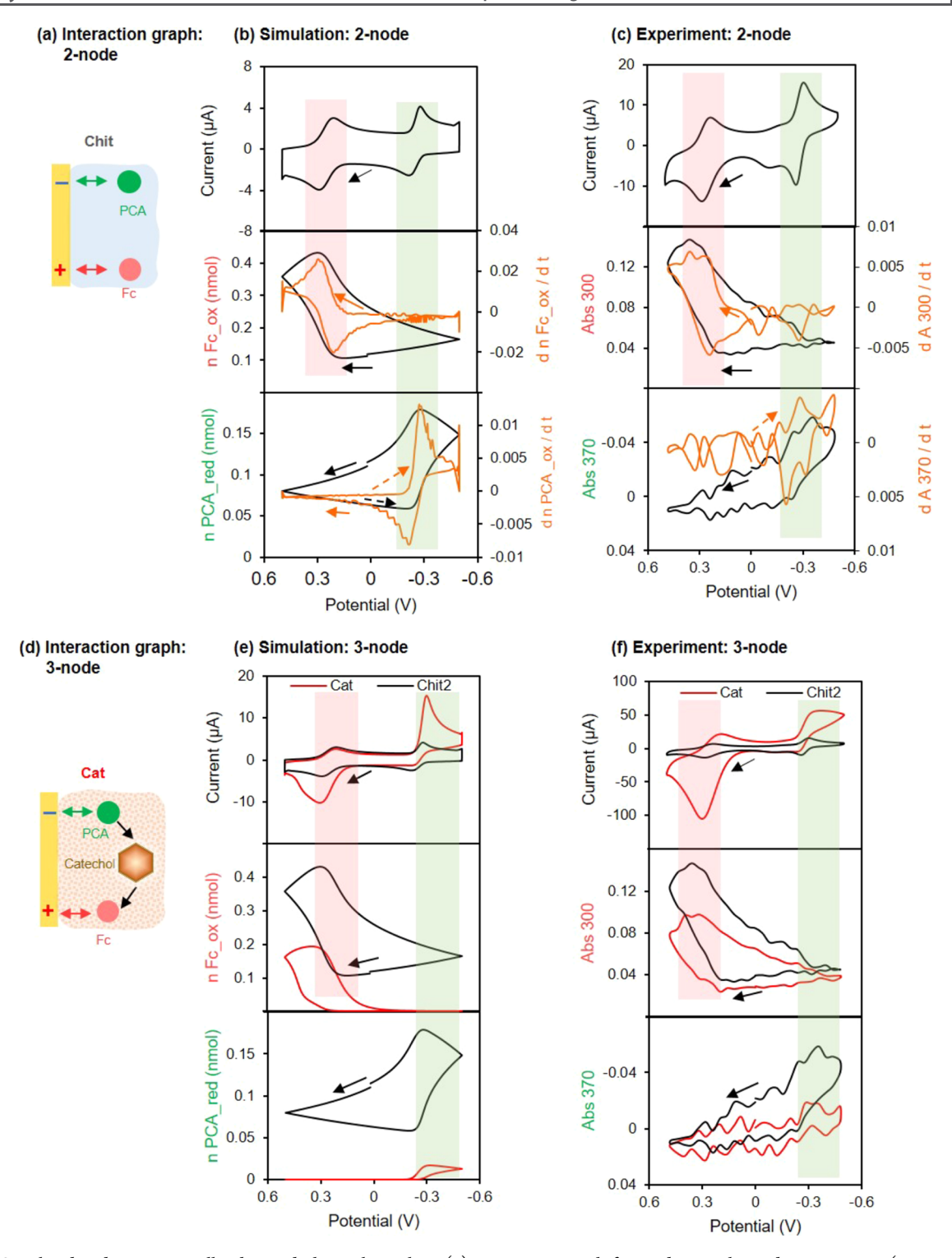


Figure 4. Simulated and experimentally observed phase plane plots. (a) Interaction graph for mediator—electrode interactions (two unconnected nodes). (b) Simulated phase plane analysis shows how the generation of the active forms of the mediators is related to the imposed potential and reveals the relationship between electrical and optical responses (note: the simulated levels of nFc^{ox} and nPCA^{red} are "proxies" for experimentally measured Abs 300 and Abs 370, respectively). (c) The experimentally observed patterns show general agreement with the simulations from the minimal deterministic model. (d) Interaction graph for the three-node network. (e) Simulations indicate that the inclusion of catechol amplifies mediator currents but attenuates the levels of their active forms (nFc^{ox} and nPCA^{red}). (f) The experimentally observed patterns show general agreement with the minimal model for this three-node network. Note: the arrows indicate the direction of scanning.

For initial simulations, we modeled interactions between the electrode and the PCA-Fc mediator pair with a cyclically oscillating imposed input potential (Figure 4a). We simulated five cycles and presented results from the last cycle. The upper

plot in Figure 4b shows the i-E phase plane plot, while the lower two curves show results for the active redox states for the individual mediators. For the Fc mediator, simulations show that the mole amount of active Fc^{ox} (nFc^{ox}) is low when the

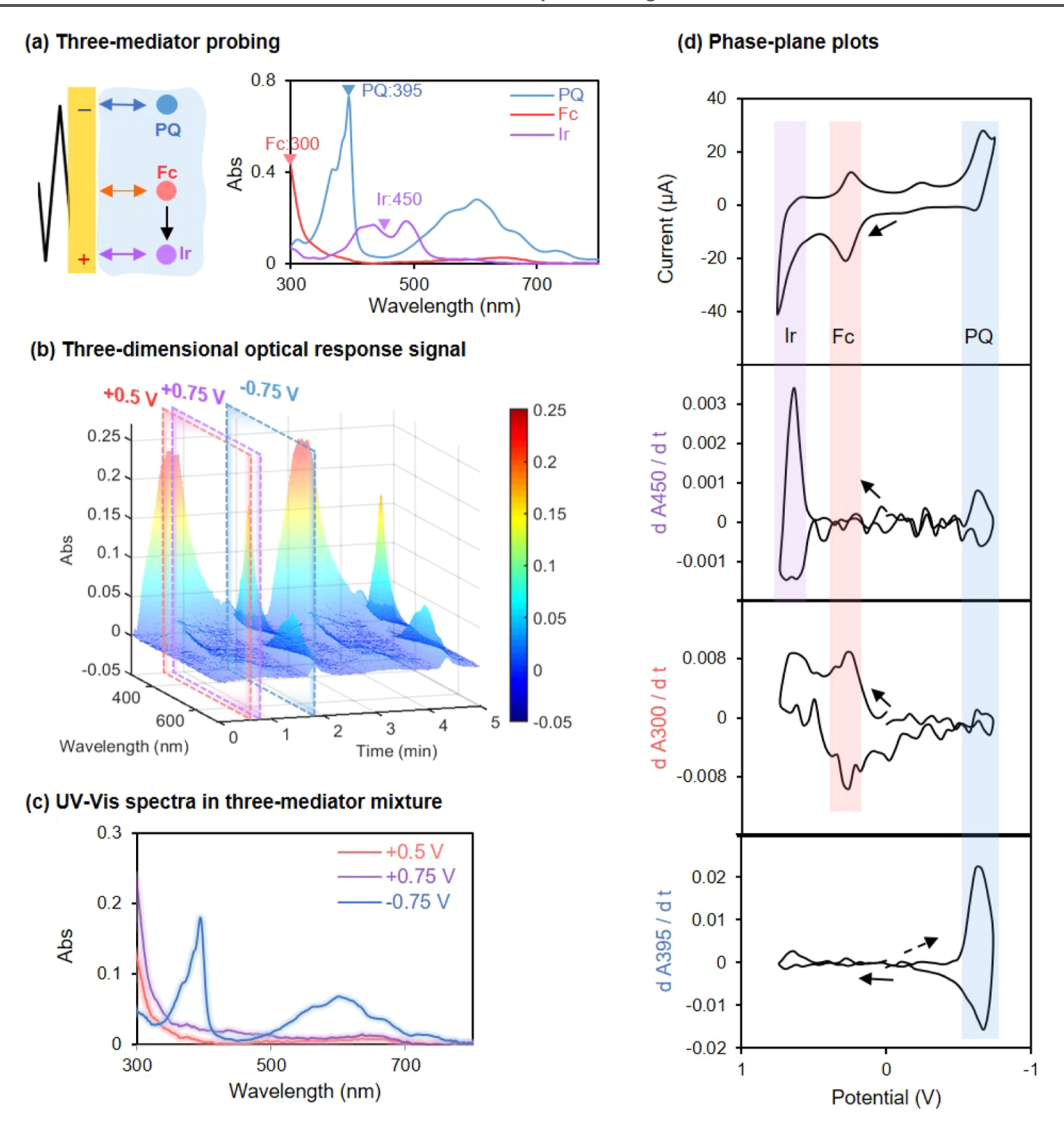


Figure 5. Redox probing of the control chitosan film with three mediators. (a) Interaction graph and redox-state-dependent optical absorbance for the individual mediators. (b) Three-dimensional plot shows the wavelength-dependent and time-dependent resolution of the absorption peaks. (c) Optical absorption spectra at three potential slices. (d) The electrical and optical response characteristics show potential-dependent changes in the current and absorbance derivatives (dAbs/dt) that are consistent with the redox-state switching of the individual mediators.

potential is scanned from reducing values (-0.5 V) to oxidizing values, until the imposed potential approaches and exceeds the E^0 value for Fc (+0.25 V). As the potential is scanned to more oxidizing E values, nFc^{ox} increases. This increase in nFc^{ox} continues even after the scan direction is reversed until it reaches approximately +0.3 V after which the amount begins decreasing. To facilitate comparison with the i-E phase plane plot, we calculated the time derivative (dnFc^{ox}/dt) or rate of appearance of Fc^{ox}. The orange-colored lines shown in Figure 4b show that the peaks of this derivative align with the current peaks in the i-E curve.

Simulations of the active form of the PCA mediator (PCA^{red}) are shown in the bottom curve of Figure 4b. As expected, these mole amounts (nPCA^{red}) remain low as the potential is scanned from oxidizing values (+0.5 V) to reducing values until the imposed potential approaches the PCA's E^0 value (-0.25 V). As the potential becomes more reducing, nPCA^{red} increases and continues increasing even after the scan direction is reversed, but then, nPCA^{red} decreases as E becomes more oxidative (i.e., more positive) than approximately -0.3 V. The time derivative of nPCA^{red} is shown in

orange, and again, the peak positions of this derivative align with the current peaks in the i-E curve.

Figure 4c shows equivalent experimental results for this PCA-Fc mediator pair observed in the final CV cycle of Figure 3. The upper i-E plot shows current peaks for the individual mediators near their respective E^0 values, and the general pattern for this electrical response curve agrees with simulations. For the optical responses, we assume that the absorbance at 300 nm (Abs 300) can be attributed to the active form of the Fc mediator Fcox and expect it to be proportional to the number of moles of Fcox near the electrode surface (note that we did not attempt to establish a quantitative relationship between Abs 300 and nFcox) [in essence, simulated nFcox can be considered to be a theorybased "proxy" for the experimentally measurable optical absorbance]. The pattern for the Abs 300 phase plane plot shows good agreement with simulations for nFcox. The time derivative of this experimental measurement shows considerable variability but generally shows the trends anticipated by simulation; that is, the peaks of these derivatives (dAbs/dt)align with the current peaks from the i-E curves.

As noted in Figure 2, the absorbance minimum at 370 nm is attributed to the active form of PCA (PCA^{red}). Specifically, the oxidized PCA shows absorbance at 370 nm, and the loss of absorbance (i.e., the negative peak) is due to the conversion of PCA^{ox} to the active form (PCA^{red}). To facilitate analysis, we reversed the y-axis scale for the Abs 370 phase plane plot. The pattern of this Abs 370 phase plane plot shows good agreement with that observed for simulated nPCA^{red}. The time derivative of this Abs 370 measurement shows even more scatter (compared to that of Abs 300), although peaks are observed that align with the i-E current peaks that are associated with PCA's oxidation and reduction.

In summary, the simulations reveal the intrinsic structure of the data (i.e., suggest the shape of the phase plane plots) and reveal relationships between the electrical and optical measurements (peaks in i and $\mathrm{dAbs}/\mathrm{d}t$). The experimentally observed patterns are consistent with these simulations and also reveal limitations to measurements. Specifically, multi-cycle input—output analysis provides insights on the reversibility of the redox reactions (by the time invariance of the signals), but such multi-cycle analysis limits the frequency where spectra can be collected due to the rate of data generation and memory requirements.

Figure 4d shows the extension of analysis to include electron exchange between the mediators and catechol. As indicated in the interaction graph, catechol can undergo directed interactions with each mediator, and the catechol node cannot directly exchange electrons with the electrode. The simulated *i*–*E* phase plane plot shown in Figure 4e shows that the addition of catechol is expected to result in amplified currents in the region of Fc oxidation and PCA reduction and partial rectifications of these currents. The simulated nFc^{ox} and nPCA^{red} phase plane plots shown in Figure 4e suggest that the addition of catechol is expected to decrease the levels of the active forms of these mediators.

The experimental phase plane plots are shown in Figure 4f, and these plots show general agreement with simulations. Specifically, the Fc oxidation currents and PCA reduction currents are amplified, while the optical absorbances associated with the active forms of the mediator are both attenuated Figure S5 of the Supporting Information compares simulated input-output curves for these electrical and optical responses with experimental observations shown in Figures 1 and 3]. Mechanistically, the current amplifications indicate that catechol leads to increases in the electrochemical generation of the active forms of the mediators, while the attenuated absorbance indicates that catechol decreases the concentrations of these active forms: these response characteristics are consistent with redox-cycling reactions between these mediators and catechol. Overall, the minimal model reveals the intrinsic structure of the data, while significant parameter optimization would be required for this model to serve as a digital replica.

Sensitivity of Response Characteristics to Network Topology. The minimal deterministic model describes how the electrical signals emerge from the networked flow of electrons through the catechol film and also how high-dimensional optical measurements can be interpreted in terms of the redox-state switching of the mediator nodes. We performed a final set of studies to extend this analysis and illustrate how the electrical and optical response characteristics vary with the redox network's topology. As illustrated in Figure 5a, we investigated a network that includes three mediators.

To assess the redox-state-dependent optical properties of these mediators, we first prepared solutions of individual mediators and used the initial absorbance of their inert forms as a baseline after which we imposed an appropriate potential for 1 min to generate their active forms and then measured their UV-vis spectra. One mediator the iridium salt K₃IrCl₆ (Ir) is commonly used for clinical analysis⁴⁸ and has a comparatively oxidative redox potential ($E^0 = +0.72 \text{ V}$). When an oxidative potential (+0.8 V) was imposed to convert the inert Irred to its active oxidized form Irox, an increase in absorbance was observed around 450 nm as illustrated by the differential absorption spectrum shown in Figure 5a. The redox-state switching of the second mediator (Fc) can be detected at 300 nm as illustrated in Figure 5a (and also Figure 3). The third mediator, paraquat (PQ), is an agricultural chemical, and because of its redox-state-dependent optical properties, it has been investigated for electronic applications (e.g., electrochromic materials⁴⁹). PQ has reductive redox potential ($E^0 = -0.64 \text{ V}$) and can accept a single electron to form a reactive free radical (PQred). After electrochemical reduction (-0.8 V; 1 min), the differential spectrum shown in Figure 5a illustrates that the generation of the active PQ^{red} can be detected at 395 nm.

In initial studies, we immersed an electrode coated with a control chitosan film into a solution containing all three mediators. Specifically, the solution contained Ir (0.4 mM), Fc (0.2 mM), and PQ (0.2 mM), and a cyclic potential input was imposed (from +0.75 to -0.75 V at a scan rate of 20 mV/s) for 10 cycles, while the optical absorbance spectrum was measured every 2 s [Figure S6 of the Supporting Information shows the input—output representation for these experiments]. Figure Sb shows the three-dimensional plot of the absorbance, wavelength, and time for the first two cycles of this time series. As can be seen, oscillating absorbance peaks are observed at several wavelengths during this potential scanning.

Although the differential spectra shown in Figure 5a show that the individual mediators have redox-state-dependent absorption peaks at specific wavelengths, these plots also suggest significant overlap in their absorption spectra. The three-dimensional plot in Figure 5b shows significant temporal separation of these spectra depending on the imposed electrode potential. This temporal (or potential)-based resolution is illustrated in Figure 5c by the two-dimensional Abs versus wavelength plots for three representative potential slices. At the characteristic wavelength for PQ absorption (i.e., 395 nm), a strong signal is observed for the reductive slice (-0.75 V), while much smaller signals appear at this wavelength for the other two potential slices. Absorption at 300 nm is observed for all three potential slices with stronger signals at the more oxidative potentials (+0.5 and +0.75 V), suggesting that all three mediators (and especially Fc and Ir) may contribute to this 300 nm signal. The absorption at 450 nm which is characteristic of the Ir mediator shows very low absorption for all three potential slices. These results indicate that the time varying spectra can provide significant insights on the dynamics of the mediators' redox-state switching; however, there are also limitations to this analysis.

The optical phase-plane analysis shown in Figure 4c indicated that further insights into the mediators' redox-state switching could be revealed from the time derivative of absorption at various wavelengths. Figure 5d shows these dAbs/dt-E phase plane plots along with the i-E phase plane plots. Analysis at 450 nm shows a large (dA450/dt) signal in

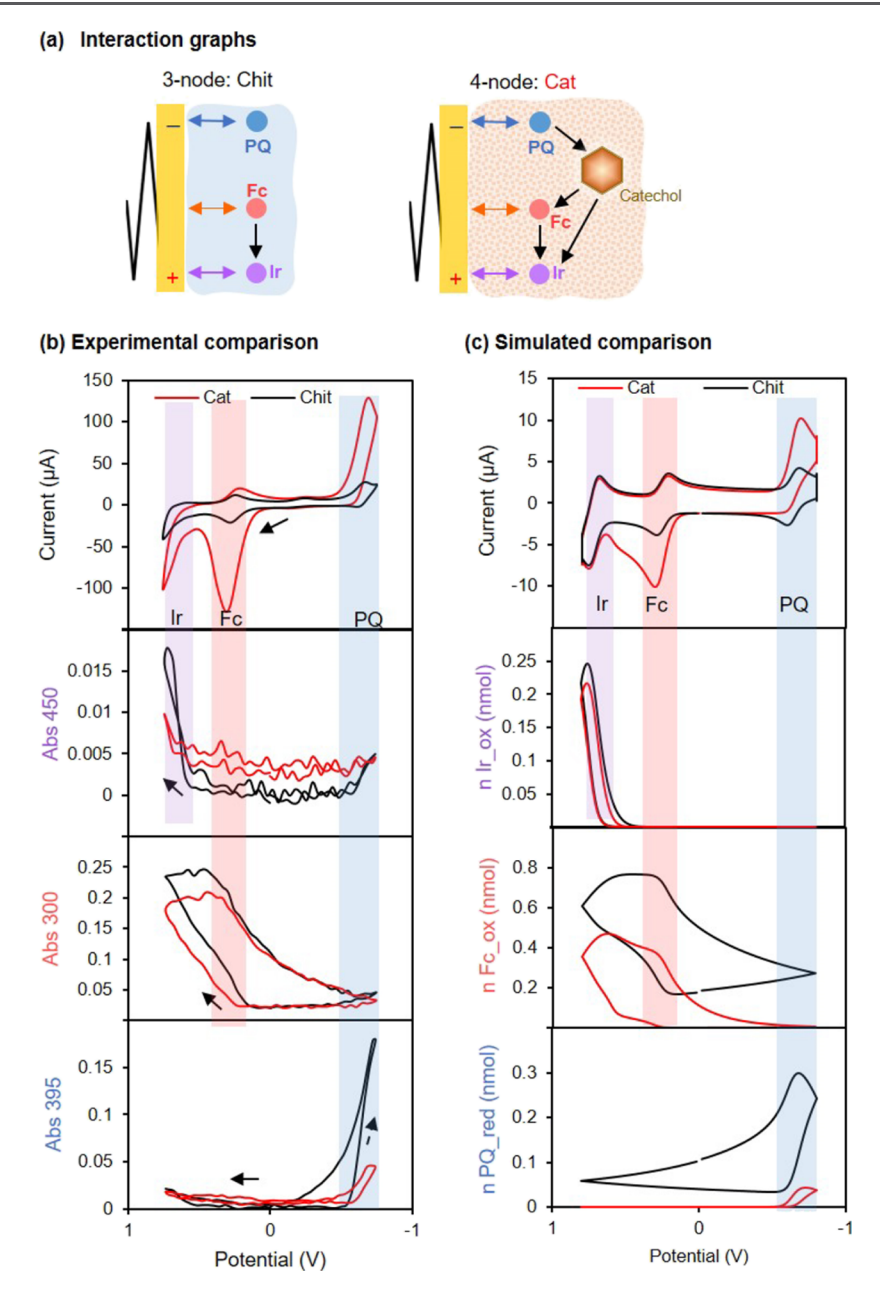


Figure 6. Comparison of the response characteristics for the catechol—chitosan and control chitosan films. (a) Interaction graphs for the three-node and four-node networks. (b) Experimental comparison of the electrical and optical response characteristics. (c) Simulations show consistent response features: the incorporation of catechol in the film amplifies currents and attenuates the levels of the active forms of the mediators (levels of the active mediators are a proxy for the experimentally observed optical absorbances).

the potential region (>+0.6 V) associated with Ir oxidation, while the small signal outside this potential region suggests little redox-state switching of Ir under more reducing conditions. Importantly, this large (dA450/dt) signal is observed despite the low absorbance observed at 450 nm shown in Figure 5c.

The (dA300/dt) signal is more complex with a comparatively stronger signal observed in the potential region associated with the Fc's E^0 value and a weaker signal in the potential region associated with the Ir's E^0 value. One hypothesis for this dA300/dt signal in the Ir- E^0 range is that this optical signal at 300 nm is the direct measurement of Ir's redox-state switching. An alternative hypothesis is that this dA300/dt signal in the Ir- E^0 range results because Fc°x is being generated through Ir–Fc mediator–mediator interactions (i.e.,

the vertical arrow in the interaction graph of Figure 5a). As detailed in the Supporting Information, both model simulations and control experiments shown in Figures S7–S11 support the conclusion that electrode-generated Ir^{ox} serves as a redox relay that can oxidize Fc^{red} that diffuses from the bulk solution.

The strong (dA395/dt) signal observed at the reducing potentials is consistent with the redox-state switching of the PQ mediator. In summary, this phase-plane analysis shows that the electrical and optical response characteristics are consistent with (or controlled by) the mediators' redox (i.e., E^0) and optical properties (i.e., the redox-state-dependent absorption).

An analogous CV experiment was performed with an electrode coated with the catechol-chitosan film, and the electrical and optical response characteristics for the catechol-

Table 2. Signal Processing Differences between Communication through Biology's Redox and Ion-Based Electrical Modalities (the Statements Are Generalizations and May Not Be Absolutely True in All Cases)

	redox modality	ion-based electrical modality
signal	often evoked (by potential and mediator inputs)	native (e.g., rhythmic electrical activity associated with a beating heart)
electrical measurement	current (e.g., Faradaic; invasive)	potential/field (non-invasive)
optical measurement	absorbance spectra (can depend on the redox state)	
signal features for system analysis	electrical (e.g., current or charge) and optical (e.g., absorbance) output responses	relative timing and peaks from time series potential measurements
system modeling framework	reaction network model (abstracted reaction-diffusion modeling)	electric circuit model (e.g., Hodgkin-Huxley)

chitosan film were compared to those for the control chitosan film (Figure 6a shows the interaction graphs for these threeand four-node networks). The experimentally observed i-Ephase plane plot shown in Figure 6b shows that in the presence of catechol, oxidative currents were amplified for the Ir and Fc mediators, and the reductive current for PQ was amplified. The experimentally observed optical phase plane plots shown in Figure 6b show that in the presence of catechol, the absorbance at all three wavelengths was attenuated (Figure S12 of the Supporting Information shows the three-dimensional plot of absorbance vs wavelength and time for these experiments). This combination of amplified currents and attenuated optical absorbance is also observed in Figure 4f and is consistent with the explanation that each mediator engages the film's grafted catechol moieties in redox-cycling reactions that shuttle electrons between the electrode and film.

Figure 6c shows simulated phase plane plots for the catechol-containing and the control films. Consistent with the experimental results shown in Figure 6b, the i-E phase plane plot shows a comparatively large amplification of Fc oxidation and a comparatively smaller amplification of the Ir oxidation. Also consistent with the experiment, the simulated *i*–*E* plot shows considerable amplification of PQ reduction. The patterns in the phase plane plots for the levels of the activated mediators (Irox, Fcox, and PQred) are also consistent with the experimental absorbance measurements. Specifically, simulations indicate that the levels of all three mediators are expected to be attenuated in the presence of catechol (compared to the control chitosan film). Thus, the minimal model captures the essential features of the potentialdependent optical and electrical signals for this more complex redox network.

DISCUSSION

Our long-term goal is to enlist the redox modality to enable bidirectional communication between biology and electronics.^{6,8} Importantly, redox is a native biological modality used for energy transduction (e.g., respiration) and communication (e.g., redox signaling), and redox is also accessible to electronics via electrochemistry. In biology, the flow of energy/ information through the redox modality involves the flow of electrons through redox reaction networks. In some cases, the redox networks are well-defined (e.g., the respiratory and photosynthetic electron transfer chains), but in other cases, they are ill-defined and dynamically changing (e.g., the redox interactomes in serum, the gut, and the rhizosphere). Importantly, many redox-active nodes are kinetically stable and do not spontaneously undergo electron transfer even when there is a thermodynamic driving force. This kinetic stability also means that many nodes cannot be readily measured by electrochemical oxidation and reduction. Thus, despite the

appeal of using redox as a modality for bio-electronic communication, there are important challenges to establishing "connectivity".

One advantage of using catechol/quinone films is that these moieties tend to have low kinetic barriers and spontaneously exchange electrons with a wide range of diffusible oxidants/ reductants: thus, catechols can facilitate redox-based bioelectronic communication as illustrated in Scheme 1b. In biology, hydroquinones/quinones are well known electron carriers in spatially organized redox networks (e.g., the respiratory and photosynthetic electron transfer chains), while emerging research is demonstrating that catechol/ quinone materials offer important redox activities in lesswell-defined networks. For instance, in vitro studies have demonstrated that natural melanins are reversibly redox-active and can undergo sustained redox cycling with drugs⁵⁰ and environmental chemicals.⁵¹ In addition, synthesized catecholbased materials can engage biology in interactive communication to upregulate biological stress responses⁵² and promote the healing of infected wounds.⁵³

In addition to exchanging electrons with biologically relevant oxidants and reductants, the catechol/quinone moieties can also exchange electrons with common electrochemical mediators. Typically, such mediators have low kinetic barriers for reversible electron exchange with an electrode. The importance of mediators is illustrated by the fact that MEP is an emerging experimental method for redox biology. ^{14,20} In MEP, the mediators serve to "transmit" electrode-imposed redox inputs; "evoke" electron-transfer interactions with nodes in the local environment; and "report" these interactions at the electrode. As suggested in Scheme 1b, we envision that the catechol moieties in the film act as hubs that significantly control the flow of electrons through the film.

In the Introduction, we compared biology's ionic-electrical and redox modalities (Table 1) and noted the success of the EKG and defibrillator for system-level sensing and actuation of biology. Table 2 further suggests differences in sensing/ actuating through biology's ionic-electrical and redox modalities. One major difference involves the electrical signal: while an EKG measures a native signal non-invasively, redox signals often must be evoked by using potential and mediator inputs to induce electron transfer reactions. From an informationprocessing perspective, the role of these inputs and the film's catechol moieties is to evoke interpretable responses that provide useful information. Previously, MEP has been used to characterize two types of redox systems: (i) well-defined systems where chemical/biological intuition can be used for interpretation ^{24,41,42,54} and (ii) ill-defined systems (e.g., serum samples) where empirical, data-driven statistical analysis is required to extract meaning from the output responses.^{26,47} In the current study, we examined defined systems of intermediate complexity to understand how measurable

features can be interpreted in terms of (i.e., mapped to) system-level network characteristics.

The important contribution of this study is increasing the dimensionality of measurement, from a single wavelength that observes the redox switching of the catechol film to the entire UV-vis spectrum that can observe the redox switching of multiple mediator nodes simultaneously. Importantly, we extended a minimal model to provide a physically realistic basis for revealing the intrinsic structure of this highdimensional data. This deterministic model supported the extension of phase plane analysis from traditional electrical measurements (e.g., current-potential; i-E) to optical measurements (absorbance-potential; Abs-E). Importantly, while the electrical measurements detect electrical activities (e.g., the evoked electron flow through the network), the optical measurements detect molecular activities (e.g., the redox-state switching of the nodes). Thus, these highdimensional optical measurements provide information that is independent from but complementary to that of the electrical measurements. In particular, the observed correlation between the i-E and (dAbs/dt) - E phase plane plots provides important insights for fusing information from orthogonal electrical and optical measurements.

CONCLUSIONS

In conclusion, we demonstrate the integration of high-dimensional optical measurements with electrical measurements for analysis of the networked flow of electrons through redox-active but non-conducting catechol hydrogel films (i.e., the films can exchange electrons with diffusible mediators but cannot directly exchange electrons with the electrode). We believe that this network analysis is a meaningful step toward a longer-term vision of redox-based bioelectronics by providing a rational basis for tuning redox inputs and interpreting output response signals. Specifically, we envision that this analysis will enhance our ability to study complex, ill-defined, and dynamically changing redox interactomes.

ASSOCIATED CONTENT

5 Supporting Information

The Supporting Information is available free of charge at https://pubs.acs.org/doi/10.1021/acs.chemmater.2c02707.

Measurement of honeycomb electrode surface area; twostep electro-fabrication of the catechol—chitosan hydrogel film; initial and differential spectra for PCA and Fc mediators; simulation geometry for the honeycomb electrode; simulated input—output time series curves for redox probing with two mediators; experimental input output time series curves for probing with three mediators; simulated results; mediator concentration profiles; phase-plane analysis; experimental evidence; three-dimensional plots of three-mediator redox probing for the control chitosan film and catechol—chitosan film; and COMSOL report (PDF)

AUTHOR INFORMATION

Corresponding Author

Gregory F. Payne — Institute for Bioscience and Biotechnology Research and Robert E. Fischell Institute for Biomedical Devices, University of Maryland, College Park, Maryland 20742, United States; ⊚ orcid.org/0000-0001-6638-9459; Email: gpayne@umd.edu

Authors

Zhiling Zhao — Institute for Bioscience and Biotechnology Research and Robert E. Fischell Institute for Biomedical Devices, University of Maryland, College Park, Maryland 20742, United States; orcid.org/0000-0003-0186-7215

Eunkyoung Kim — Institute for Bioscience and Biotechnology Research and Robert E. Fischell Institute for Biomedical Devices, University of Maryland, College Park, Maryland 20742, United States; © orcid.org/0000-0003-2566-4041

Dana Motabar – Institute for Bioscience and Biotechnology Research, Robert E. Fischell Institute for Biomedical Devices, and Fischell Department of Bioengineering, University of Maryland, College Park, Maryland 20742, United States

William E. Bentley — Institute for Bioscience and Biotechnology Research, Robert E. Fischell Institute for Biomedical Devices, and Fischell Department of Bioengineering, University of Maryland, College Park, Maryland 20742, United States; orcid.org/0000-0002-4855-7866

Complete contact information is available at: https://pubs.acs.org/10.1021/acs.chemmater.2c02707

Notes

The authors declare no competing financial interest.

ACKNOWLEDGMENTS

This work was supported by the National Science Foundation (CBET#1932963), the Defense Threat Reduction Agency (HDTRA1-19-0021), and the Department of Energy, OBER, Lawrence Livermore National Laboratory SFA (under contract DE-AC52-07NA27344, LLNL-JRNL-827946).

■ REFERENCES

- (1) Tatinclaux, M.; Gregoire, K.; Leininger, A.; Biffinger, J. C.; Tender, L.; Ramirez, M.; Torrents, A.; Kjellerup, B. V. Electricity Generation from Wastewater Using a Floating Air Cathode Microbial Fuel Cell. *Water-Energy Nexus* **2018**, *1*, 97–103.
- (2) Li, J.; Wu, S.; Kim, E.; Yan, K.; Liu, H.; Liu, C.; Dong, H.; Qu, X.; Shi, X.; Shen, J.; Bentley, W. E.; Payne, G. F. Electrobiofabrication: Electrically Based Fabrication with Biologically Derived Materials. *Biofabrication* **2019**, *11*, 032002.
- (3) Lai, B.; Glaven, S.; Song, H. Electrobiotechnology Towards Sustainable Bioeconomy: Fundamental, Optimization and Applications. *Front. Bioeng. Biotechnol.* **2022**, *10*, 901072.
- (4) Bird, L. J.; Kundu, B. B.; Tschirhart, T.; Corts, A. D.; Su, L.; Gralnick, J. A.; Ajo-Franklin, C. M.; Glaven, S. M. Engineering Wired Life: Synthetic Biology for Electroactive Bacteria. *ACS Synth. Biol.* **2021**, *10*, 2808–2823.
- (5) Mansouri, M.; Fussenegger, M. Electrogenetics: Bridging Synthetic Biology and Electronics to Remotely Control the Behavior of Mammalian Designer Cells. *Curr. Opin. Chem. Biol.* **2022**, *68*, 102151.
- (6) VanArsdale, E.; Pitzer, J.; Payne, G. F.; Bentley, W. E. Redox Electrochemistry to Interrogate and Control Biomolecular Communication. *Iscience* **2020**, 23, 101545.
- (7) Krawczyk, K.; Xue, S.; Buchmann, P.; Charpin-El-Hamri, G.; Saxena, P.; Hussherr, M. D.; Shao, J.; Ye, H.; Xie, M.; Fussenegger, M. Electrogenetic Cellular Insulin Release for Real-Time Glycemic Control in Type 1 Diabetic Mice. *Science* **2020**, *368*, 993–1001.
- (8) Kim, E.; Li, J.; Kang, M.; Kelly, D. L.; Chen, S.; Napolitano, A.; Panzella, L.; Shi, X.; Yan, K.; Wu, S.; Shen, J.; Bentley, W. E.; Payne, G. F. Redox Is a Global Biodevice Information Processing Modality. *Proc. IEEE* **2019**, *107*, 1402–1424.
- (9) Liu, Y.; Li, J.; Tschirhart, T.; Terrell, J. L.; Kim, E.; Tsao, C. Y.; Kelly, D. L.; Bentley, W. E.; Payne, G. F. Connecting Biology to

Electronics: Molecular Communication via Redox Modality. *Adv. Healthc. Mater.* **2017**, *6*, 1700789.

- (10) Liu, Y. L.; Huang, W. H. Stretchable Electrochemical Sensors for Cell and Tissue Detection. *Angew. Chem., Int. Ed.* **2020**, *60*, 2757–2767.
- (11) Wu, W.; Chen, X.; Jiao, Y.; Fan, W.; Liu, Y.; Huang, W. Versatile Construction of Biomimetic Nanosensors for Electrochemical Monitoring of Intracellular Glutathione. *Angew. Chem., Int. Ed.* **2022**, *61*, No. e202115820.
- (12) Shaver, A.; Arroyo-Currás, N. The Challenge of Long-Term Stability for Nucleic Acid-Based Electrochemical Sensors. *Curr. Opin. Electrochem.* **2022**, 32, 100902.
- (13) Wu, Y.; Arroyo-Currás, N. Advances in Nucleic Acid Architectures for Electrochemical Sensing. *Curr. Opin. Electrochem.* **2021**, *27*, 100695.
- (14) Zhao, Z.; Ozcan, E. E.; VanArsdale, E.; Li, J.; Kim, E.; Sandler, A. D.; Kelly, D. L.; Bentley, W. E.; Payne, G. F. Mediated Electrochemical Probing: A Systems-Level Tool for Redox Biology. *ACS Chem. Biol.* **2021**, *16*, 1099–1110.
- (15) Matthews, J. D.; Reedy, A. R.; Wu, H.; Hinrichs, B. H.; Darby, T. M.; Addis, C.; Robinson, B. S.; Go, Y. M.; Jones, D. P.; Jones, R. M.; Neish, A. S. Proteomic Analysis of Microbial Induced Redox-Dependent Intestinal Signaling. *Redox Biol.* **2019**, *20*, 526–532.
- (16) Timme-Laragy, A. R.; Hahn, M. E.; Hansen, J. M.; Rastogi, A.; Roy, M. A. Redox Stress and Signaling during Vertebrate Embryonic Development: Regulation and Responses. *Semin. Cell Dev. Biol.* **2018**, 80, 17–28.
- (17) Jones, D. P.; Sies, H. The Redox Code. *Antioxid. Redox Signal.* **2015**, 23, 734–746.
- (18) Cortese-Krott, M. M.; Koning, A.; Kuhnle, G. G. C.; Nagy, P.; Bianco, C. L.; Pasch, A.; Wink, D. A.; Fukuto, J. M.; Jackson, A. A.; van Goor, H.; Olson, K. R.; Feelisch, M. The Reactive Species Interactome: Evolutionary Emergence, Biological Significance, and Opportunities for Redox Metabolomics and Personalized Medicine. *Antioxidants Redox Signal.* 2017, 27, 684–712.
- (19) Santolini, J.; Wootton, S. A.; Jackson, A. A.; Feelisch, M. The Redox Architecture of Physiological Function. *Curr. Opin. Physiol.* **2019**, *9*, 34–47.
- (20) Motabar, D.; Li, J.; Payne, G. F.; Bentley, W. E. Mediated Electrochemistry for Redox-Based Biological Targeting: Entangling Sensing and Actuation for Maximizing Information Transfer. *Curr. Opin. Biotechnol.* **2021**, *71*, 137–144.
- (21) Kim, E.; Kang, M.; Tschirhart, T.; Malo, M.; Dadachova, E.; Cao, G.; Yin, J. J.; Bentley, W. E.; Wang, Z.; Payne, G. F. Spectroelectrochemical Reverse Engineering DemonstratesThat Melanin's Redox and Radical Scavenging Activities Are Linked. *Biomacromolecules* **2017**, *18*, 4084–4098.
- (22) Scheller, F. W.; Schubert, F.; Neumann, B.; Pfeiffer, D.; Hintsche, R.; Dransfeld, I.; Wollenberger, U.; Renneberg, R.; Warsinke, A.; Johansson, G.; Skoog, M.; Yang, X.; Bogdanovskaya, V.; Bückmann, A.; Zaitsev, S. Y. Second Generation Biosensors. *Biosens. Bioelectron.* 1991, 6, 245–253.
- (23) Fultz, M. L.; Durst, R. A. Mediator Compounds for the Electrochemical Study of Biological Redox Systems: A Compilation. *Anal. Chim. Acta* **1982**, *140*, 1–18.
- (24) Hu, K.; Liu, Y. L.; Oleinick, A.; Mirkin, M. V.; Huang, W. H.; Amatore, C. Nanoelectrodes for Intracellular Measurements of Reactive Oxygen and Nitrogen Species in Single Living Cells. *Curr. Opin. Electrochem.* **2020**, 22, 44–50.
- (25) Rabinowitz, J. D.; Vacchino, J. F.; Beeson, C.; McConnell, H. M. Potentiometric Measurement of Intracellular Redox Activity. J. Am. Chem. Soc. 1998, 120, 2464–2473.
- (26) Kang, M.; Kim, E.; Chen, S.; Bentley, W. E.; Kelly, D. L.; Payne, G. F. Signal Processing Approach to Probe Chemical Space for Discriminating Redox Signatures. *Biosens. Bioelectron.* **2018**, *112*, 127–135.
- (27) Chen, W.; Yu, A.; Sun, Z.-J.; Zhu, B.-Q.; Cai, J.; Chen, Y.-X. Probing Complex Eletrocatalytic Reactions Using Electrochemical Infrared Spectroscopy. *Curr. Opin. Electrochem.* **2019**, *14*, 113–123.

- (28) Kaim, W.; Fiedler, J. Spectroelectrochemistry: The Best of Two Worlds. *Chem. Soc. Rev.* **2009**, *38*, 3373–3382.
- (29) Zhai, Y.; Zhu, Z.; Zhou, S.; Zhu, C.; Dong, S. Recent Advances in Spectroelectrochemistry. *Nanoscale* **2018**, *10*, 3089–3111.
- (30) Lozeman, J. J. A.; Führer, P.; Olthuis, W.; Odijk, M. Spectroelectrochemistry, the Future of Visualizing Electrode Processes by Hyphenating Electrochemistry with Spectroscopic Techniques. *Analyst* **2020**, *145*, 2482–2509.
- (31) Bond, A. M.; Zhang, J.; Gundry, L.; Kennedy, G. F. Opportunities and Challenges in Applying Machine Learning to Voltammetric Mechanistic Studies. *Curr. Opin. Electrochem.* **2022**, 34, 101009.
- (32) Gundry, L.; Kennedy, G.; Bond, A. M.; Zhang, J. Inclusion of Multiple Cycling of Potential in the Deep Neural Network Classification of Voltammetric Reaction Mechanisms. *Faraday Discuss.* **2022**, 233, 44–57.
- (33) Cannan, S.; Cervera, J.; Steliaros, R. J.; Bitziou, E.; Whitworth, A. L.; Unwin, P. R. Scanning Electrochemical Microscopy (SECM) Studies of Catalytic EC' Processes: Theory and Experiment for Feedback, Generation/Collection and Imaging Measurements. *Phys. Chem. Chem. Phys.* **2011**, *13*, 5403–5412.
- (34) Feldberg, S. W.; Campbell, J. F. The Quasicatalytic Mechanism: A Variation of the Catalytic (EC') Mechanism. *Anal. Chem.* **2009**, *81*, 8797–8800.
- (35) Wu, S.; Kim, E.; Li, J.; Bentley, W. E.; Shi, X.-W.; Payne, G. F. Catechol-Based Capacitor for Redox-Linked Bioelectronics. *ACS Appl. Electron. Mater.* **2019**, *1*, 1337–1347.
- (36) Wu, S.; Kim, E.; Chen, C.; Li, J.; VanArsdale, E.; Grieco, C.; Kohler, B.; Bentley, W. E.; Shi, X.; Payne, G. F. Catechol-Based Molecular Memory Film for Redox Linked Bioelectronics. *Adv. Electron. Mater.* **2020**, *6*, 2000452.
- (37) Wu, S.; Zhao, Z.; Rzasa, J. R.; Kim, E.; Li, J.; VanArsdale, E.; Bentley, W. E.; Shi, X.; Payne, G. F. Hydrogel Patterning with Catechol Enables Networked Electron Flow. *Adv. Funct. Mater.* **2021**, *31*, 2007709.
- (38) Ding, T.; Wang, Z.; Xia, D.; Zhu, J.; Huang, J.; Xing, Y.; Wang, S.; Chen, Y.; Zhang, J.; Cai, K. Long-Lasting Reactive Oxygen Species Generation by Porous Redox Mediator-Potentiated Nanoreactor for Effective Tumor Therapy. *Adv. Funct. Mater.* **2021**, *31*, 2008573.
- (39) Yang, M.; Wang, Z.; Ding, T.; Tang, J.; Xie, X.; Xing, Y.; Wang, L.; Zhang, J.; Cai, K. Interfacial Engineering of Hybrid Polydopamine/Polypyrrole Nanosheets with Narrow Band Gaps for Fluorescence Sensing of MicroRNA. ACS Appl. Mater. Interfaces 2021, 13, 42183–42194.
- (40) Kim, E.; Liu, Y.; Shi, X. W.; Yang, X.; Bentley, W. E.; Payne, G. F. Biomimetic Approach to Confer Redox Activity to Thin Chitosan Films. *Adv. Funct. Mater.* **2010**, *20*, 2683–2694.
- (41) Kim, E.; Gordonov, T.; Bentley, W. E.; Payne, G. F. Amplified and in Situ Detection of Redox-Active Metabolite Using a Biobased Redox Capacitor. *Anal. Chem.* **2013**, *85*, 2102–2108.
- (42) Liu, Y.; Tsao, C. Y.; Kim, E.; Tschirhart, T.; Terrell, J. L.; Bentley, W. E.; Payne, G. F. Using a Redox Modality to Connect Synthetic Biology to Electronics: Hydrogel-Based Chemo-Electro Signal Transduction for Molecular Communication. *Adv. Healthc. Mater.* **2017**, *6*, 1600908.
- (43) Zhao, Z.; Wu, S.; Kim, E.; Chen, C.; Rzasa, J. R.; Shi, X.; Bentley, W. E.; Payne, G. F. System-Level Network Analysis of a Catechol Component for Redox Bioelectronics. *ACS Appl. Electron. Mater.* **2022**, *4*, 2490–2501.
- (44) Piechota, E. J.; Troian-Gautier, L.; Sampaio, R. N.; Brennaman, M. K.; Hu, K.; Berlinguette, C. P.; Meyer, G. J. Optical Intramolecular Electron Transfer in Opposite Directions through the Same Bridge That Follows Different Pathways. *J. Am. Chem. Soc.* **2018**, *140*, 7176–7186.
- (45) Hameed, A.; Pi, H.; Lin, S.; Lai, W.; Young, L.; Liu, Y.; Shen, F.; Young, C. Direct Electrochemical Sensing of Phenazine-1-carboxylic Acid Secreted by Pseudomonas Chlororaphis Subsp. Aureofaciens BCRC 11057T Using Disposable Screen-printed Carbon Electrode. *Electroanalysis* 2016, 28, 846–853.

- (46) Cao, C.; Kim, E.; Liu, Y.; Kang, M.; Li, J.; Yin, J. J.; Liu, H.; Qu, X.; Liu, C.; Bentley, W. E.; Payne, G. F. Radical Scavenging Activities of Biomimetic Catechol-Chitosan Films. *Biomacromolecules* **2018**, *19*, 3502–3514.
- (47) Kim, E.; Zhao, Z.; Rzasa, J. R.; Glassman, M.; Bentley, W. E.; Chen, S.; Kelly, D. L.; Payne, G. F. Association of Acute Psychosocial Stress with Oxidative Stress: Evidence from Serum Analysis. *Redox Biol.* **2021**, *47*, 102138.
- (48) Kim, E.; Keskey, Z.; Kang, M.; Kitchen, C.; Bentley, W. E.; Chen, S.; Kelly, D. L.; Payne, G. F. Validation of Oxidative Stress Assay for Schizophrenia. *Schizophr. Res.* **2019**, 212, 126–133.
- (49) Madasamy, K.; Velayutham, D.; Suryanarayanan, V.; Kathiresan, M.; Ho, K.-C. Viologen-Based Electrochromic Materials and Devices. *J. Mater. Chem. C* **2019**, *7*, 4622–4637.
- (50) Temoçin, Z.; Kim, E.; Li, J.; Panzella, L.; Alfieri, M.; Napolitano, A.; Kelly, L. D.; Payne, E. W.; Payne, F. G. The Analgesic Acetaminophen and the Antipsychotic Clozapine Can Each Redox-Cycle with Melanin. ACS Chem. Neurosci. 2017, 8, 2766–2777.
- (51) Kim, E.; Leverage, W. T.; Liu, Y.; Panzella, L.; Alfieri, M. L.; Napolitano, A.; Bentley, W. E.; Payne, G. F. Paraquat-Melanin Redox-Cycling: Evidence from Electrochemical Reverse Engineering. *ACS Chem. Neurosci.* **2016**, *7*, 1057–1067.
- (52) Li, J.; Wang, S. P.; Zong, G.; Kim, E.; Tsao, C.-Y.; VanArsdale, E.; Wang, L. X.; Bentley, W. E.; Payne, G. F. Interactive Materials for Bidirectional Redox-Based Communication. *Adv. Mater.* **2021**, *33*, 2007758.
- (53) Liu, H.; Qu, X.; Kim, E.; Lei, M.; Dai, K.; Tan, X.; Xu, M.; Li, J.; Liu, Y.; Shi, X.; Li, P.; Payne, G. F.; Liu, C. Bio-Inspired Redox-Cycling Antimicrobial Film for Sustained Generation of Reactive Oxygen Species. *Biomaterials* **2018**, *162*, 109–122.
- (54) Liu, B.; Rotenberg, S. A.; Mirkin, M. V. Scanning Electrochemical Microscopy of Living Cells: Different Redox Activities of Nonmetastatic and Metastatic Human Breast Cells. *Proc. Natl. Acad. Sci. U.S.A.* **2000**, *97*, 9855–9860.

☐ Recommended by ACS

Evaluating the Catalytic Efficiency of the Human Membrane-type 1 Matrix Metalloproteinase (MMP-14) Using AuNP-Peptide Conjugates

Zhicheng Jin, Hedi Mattoussi, et al.

FEBRUARY 20, 2023

JOURNAL OF THE AMERICAN CHEMICAL SOCIETY

RFAD 🗹

"Clickable" Organic Electrochemical Transistors

Gonzalo E. Fenoy, Wolfgang Knoll, et al.

NOVEMBER 23, 2022

JACS AU

READ 🗹

Experimental Data Confirm Carrier-Cascade Model for Solid-State Conductance across Proteins

Eszter Papp, David Cahen, et al.

FEBRUARY 15, 2023

THE JOURNAL OF PHYSICAL CHEMISTRY B

READ 🗹

Light-Induced Patterning of Electroactive Bacterial Biofilms

Fengjie Zhao, James Q. Boedicker, et al.

JUNE 22, 2022

ACS SYNTHETIC BIOLOGY

READ 🗹

Get More Suggestions >